Self-Triggering High-Frequency Nanosecond Pulse Generator

Weirong Zeng, Chenguo Yao, *Member, IEEE*, Shoulong Dong, *Member, IEEE*, Yilin Wang, Jianhao Ma, *Student Member, IEEE*, Yingjiang He, and Liang Yu, *Member, IEEE*

***Abstract*—With the increasingly extensive and in-depth applications of all solid-state high-voltage nanosecond pulse generators in the defense and industrial fields, the development of traditional pulse generators faces many key issues, such as high-voltage drive isolation, compact design, and reduced weight. Hence, a novel circuit topology for a self-triggered high-frequency nanosecond pulse generator is proposed. Through high potential energy-gaining technology of the interstage capacitance, this generator does not need a complicated metal–oxide–semiconductor field-effect transistor isolation drive circuit, and there are also no switching dynamic and static voltage equalization problems. This kind of generator is very suitable for compact assembly with only a single external gate driver. High voltage output can be realized by quantizing multilevel module stacking according to actual needs. At the same time, the generator has a high repetition rate and long life. The characteristic parameters of the 20-stage superposition experimental prototype are as follows: an output voltage amplitude of 15.3 kV with a rising time of approximately 45 ns, a repetition rate of 10 kHz in the pulse train, and a pulsewidth of 200–1000 ns.**

***Index Terms*—Drive isolation, high frequency, high voltage, Marx, pulse generator, self-triggering.**

I. Introduction

With the development of active flow control technology, nanosecond pulse dielectric barrier discharge plasma flow control has attracted great attention worldwide. The plasma is formed by ionizing air, which injects momentum or energy into the air to achieve the effect of flow control [1]–[3]. This method has advantages of small size, low weight, quick response, wide-band control performance, etc., and has broad application prospects for improving the aerodynamic characteristics of aircraft/engines [4], [5].

Manuscript received August 28, 2019; revised November 19, 2019; accepted January 12, 2020. Date of publication January 15, 2020; date of current version April 22, 2020. This work was supported in part by the National Natural Science Foundation of China under Grants 51807016 and 51877022, and in part by the Postdoctoral Fund Project of Chongqing under Grant XmT2018012. Recommended for publication by Associate Editor J. Clare. *(Corresponding author: Shoulong Dong.)*

W. Zeng, C. Yao, Y. Wang, J. Ma, Y. He, and L. Yu are with the State Key Laboratory of Power Transmission Equipment & System Security and New Technology, Chongqing University, Chongqing 400044, China (e-mail: zengweirong@cqu.edu.cn; yaochenguo@cqu.edu.cn; wangyilin@cqu.edu.cn; majianhao@cqu.edu.cn; heyingjiang@cqu.edu.cn; yu_liang@cqu.edu.cn).

S. Dong is with the State Key Laboratory of Power Transmission Equipment & System Security and New Technology, Chongqing University, Chongqing 400044, China, and also with the Electrical Engineering Postdoctoral Mobile Station, Chongqing University, Chongqing 400044, China (e-mail: dsl@cqu.edu.cn).

Color versions of one or more of the figures in this article are available online at https://ieeexplore.ieee.org.

Digital Object Identifier 10.1109/TPEL.2020.2967183

A nanosecond pulse generator is a common excitation power supply for plasma flow control [2], [3]. However, nanosecond pulse generators based on traditional devices, such as spark gap switching and magnetic switching, can no longer meet the demand for plasma flow control. Therefore, the development of a nanosecond pulse generator with a higher voltage amplitude (∼tens of kV or even higher), smaller volume, lower weight, and more stable square/quasi-square waveform with a full width at half maximum of tens of nanoseconds to hundreds of nanoseconds and high repetition frequency (0–10 kHz or even higher) is of great significance to improve the flow control effect in complex environments with high-speed and high-pressure flows [2], [3], [6], [7].

With the continuous development of power electronics technology, nanosecond pulse sources based on all solid-state devices are expected to provide pulse generators that meet the requirements of this application field. At present, the high-voltage nanosecond pulse circuit topology mainly includes pulse-forming lines (PFLs) [8]–[10], Marx circuits [11]–[14], modular multilevel converters [15], [16], linear transformer drivers (LTDs) [17], [18], etc. The PFL generator can only adjust the pulsewidth by changing the length of the transmission line and requires load impedance matching with poor flexibility [9]. Marx circuits can avoid some shortcomings of the PFL, but the driving circuit of the switches requires high withstand voltage isolation since the switches operate at different potentials during the discharge duration. Generally, one of the commonly isolated methods is to use an isolated dc–dc power supply module to supply power to the drive circuit [11], [19], [20], and the other is to use a drive transformer to directly provide gate drive [21]–[23]. However, the use of isolated power modules has an adverse effect on the compactness, miniaturization, and cost control of the device since it is usually very expensive and these isolated modules commonly available on the market have a maximum limited isolation voltage. If a higher amplitude pulse voltage is required, the withstand voltages of isolated modules are limited, which causes the bottleneck problem to remain. On the other hand, the use of a driving transformer will deteriorate the leading edge characteristics of the drive signal, and the precise synchronization of trigger signals at all levels cannot be ensured. Moreover, the entire system will become more cumbersome.

Wang *et al.* [24] used a high-ratio pulse transformer to boost the lower voltage of the Marx output to directly obtain a high-gain voltage pulse. However, it is undeniable that the pulse

transformer not only has a magnetic flux reset problem [25] but also the stray capacitance and inductance of the transformer will lead to a distortion of the pulse waveform. Pang *et al.* [26] used a plurality of metal–oxide–semiconductor field-effect transistors (MOSFETs) to directly form self-triggering high-voltage switches in series. Additionally, a higher pulse voltage output was obtained by a three-stage Marx superposition consisting of this high-voltage switch, which reduces the number of driving transformers. However, this kind of topology has the problem of a dynamic unbalanced switching voltage and requires an expensive high-voltage dc power supply with low voltage gain.

Compared with the Marx circuits, the LTD is equivalent to a transformer with a turn ratio of 1:1, and all the switching control circuits share the same ground potential [27]. Therefore, it is theoretically possible to achieve an unrestricted superposition of the series without the drive isolation withstand voltage limitation. Similarly, due to the presence of the magnetic core, the size and weight of the pulse source cannot be further compressed, limiting its range of applications.

In [28] and [29], avalanche transistors were used to achieve a subnanosecond pulse output with a high voltage gain through a Marx circuit. Although there is no driving isolation problem, the avalanche transistor has low current-passing capacity and poor circuit stability, so it is less used in high-power applications.

To solve the aforementioned problems, a novel self-triggering high-voltage nanosecond pulse generator similar to an avalanche transistor circuit is proposed in this article. The main circuit still uses the classic Marx circuit topology, but only one gate drive signal of the lowest stage is required, and this driver does not require high voltage isolation. For the other levels of this circuit, high potential-energy-gaining technology based on the interstage capacitor is applied to trigger the corresponding MOSFET of the other levels in turn. Therefore, this topology avoids using complex isolated driving circuits, which greatly reduces the size and weight of the entire device. Additionally, all switches in the circuit are subjected to an equal voltage, and there are no dynamic and static voltage sharing problems under switching transients, which is of great significance for ensuring switches' long-term reliability and stable operation. Theoretically, this novel Marx topology can be extended to any level to obtain a high-voltage gain pulse output.

In this article, first, three different energy-gaining methods based on interstage capacitors are compared. Then, the operating principle of the novel pulse generator is described, and the parameter selection criteria of the corresponding passive/active devices are derived. Finally, a 20-stage experimental prototype is designed. The maximum output pulse amplitude of the prototype can reach 15.3 kV with a rising time of approximately 45 ns, the pulsewidth being 200–1000 ns, and the frequency within the output pulse train can reach 10 kHz.

II. Topology and Operation of the Proposed Self-Triggering Marx Generator

Depending on the different connections among the stages of the energy-gaining capacitor, three different self-triggering Marx generator topologies can be derived, as shown in Fig. 1.

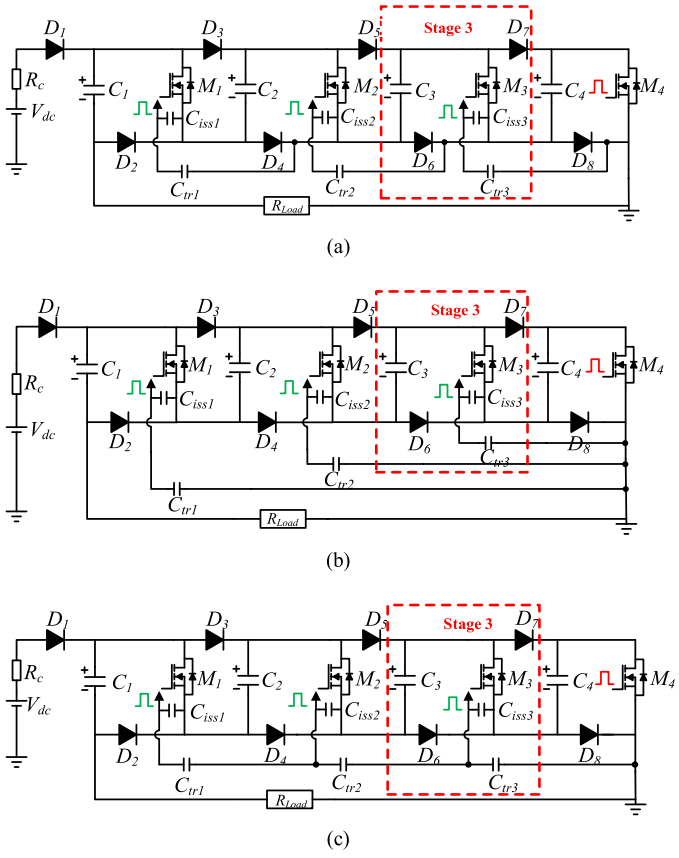

Fig. 1. Self-triggering Marx topology.

All three kinds of topologies have a remarkable advantage, that is, the multistage Marx requires only one gate driver and this driver does not require high voltage isolation. It can obtain a high-voltage pulse output by multistage superposition without complicated isolation drive circuits.

It is undeniable that there are certain differences among the three topologies. For topology (b), on the one hand, when the number of superimposed stages increases, the operating voltage of the energy-gaining capacitor increases. In addition, the value of the energy-gaining capacitor is approximately several picofarads, which gradually decreases with increasing stages. It can be predicted that the selected parameters will be more sensitive to the stray parameters of the circuit. Although topology (c) can overcome the limitation of the capacitance withstanding voltage, the sequential series connection of the energy-gaining capacitor can not only cause mutual coupling among the triggering circuit, affecting the pulse front time, but also increase the stray inductance of the triggering circuit. This increase will lead to a large oscillation of the gate voltage and the drain–source voltage if the circuit layout is not compact enough, which makes the switch susceptible to damage.

Clearly, topology (a) does not have the drawbacks of the above two topologies. Therefore, a detailed analysis of the working principle of topology (a) with four stages will be conducted. There are three different operating modes by controlling the switching stage of the first stage as follows.

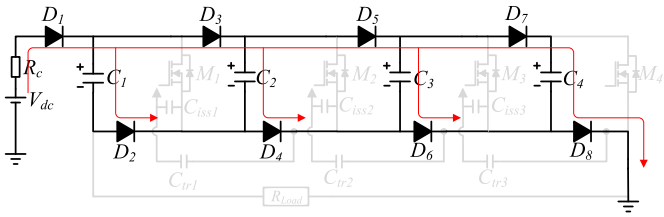

Fig. 2. Charging mode.

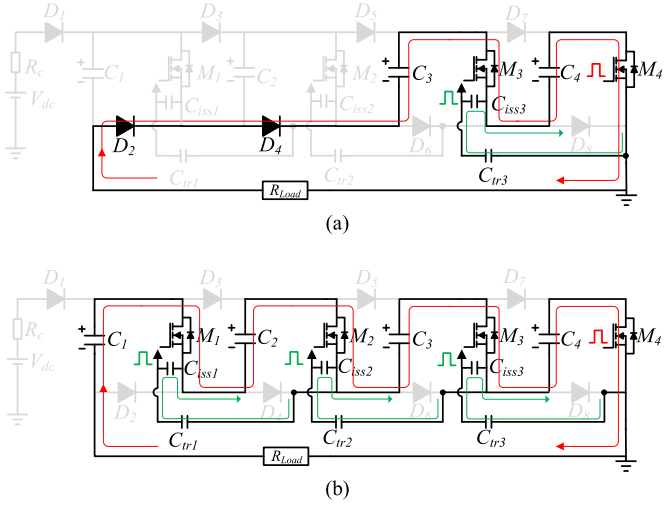

Fig. 3. (a) Turn-ON transient state under a resistive load. (b) Discharge mode under a resistive load.

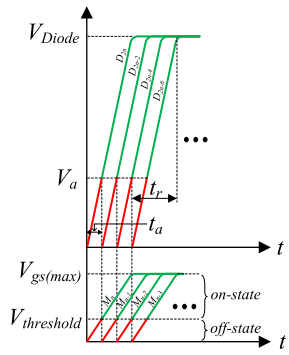

Fig. 4. Voltage diagram of V_{Ciss} and V_{diode}.

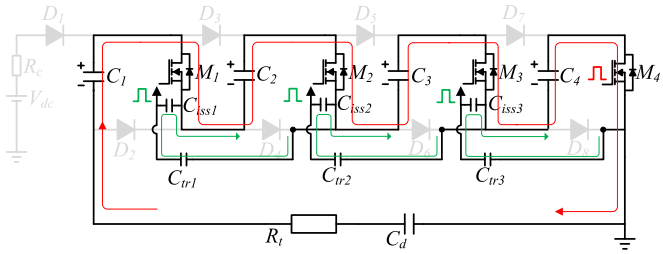

Fig. 5. Discharge mode under a capacitive load.

A. Mode I

The generator operates in the charging mode, as shown in Fig. 2. Switch M_4 is open, and then the remaining MOSFETs of every stage will transit into the OFF state. When reaching steady state, the energy storage capacitor's voltage is the same as the charge voltage V_{dc}; hence, the output voltage is zero.

B. Mode II

The generator works in the discharge mode. First, taking the resistive load as an example, as shown in Fig. 3(a), the energy storage capacitor C_4 of the first stage discharges to R_{Load} when switch M_4 is closed. Consequently, the equivalent input capacitor C_{iss3} of M_3 and the energy-gaining capacitor C_{tr3} will be charged by capacitor C_4. When M_4 is in the ON state, the junction capacitance of D_8, C_{tr3}–C_{iss3}, and C_4 are connected in parallel. Moreover, the junction capacitance of D_8 is at a picoferad level, which is much smaller than C_4, so the charge draining by the junction capacitance is negligible. As shown in Fig. 4, V_{Ciss3} will reach the threshold voltage after a delay time of t_a. Therefore, M_3 will turn ON immediately. Similarly, M_2 and M_1 will transit into the ON state in sequence, as shown in Fig. 3(b). R_{c} is the discharge protection resistor, which can also be replaced by an inductor to protect the high-voltage dc power supply.

The type of load of the dielectric barrier discharge plasma flow control application is capacitive, which can be equivalent to the series connection of capacitors C_d and R_t, as shown in Fig. 5. It can be seen from the figure that the self-triggering process is not affected by the capacitive load since there is no direct electrical coupling between the triggering circuit of each stage and the load, which is consistent with the resistive load.

If the capacitor C_1–C_4 voltage drop is within the controllable range during the discharge process, then all switches are guaranteed to be turned ON steadily, and the voltage on the load is

$$V_{\mathrm{Load}} = 4V_{\mathrm{dc}}.$$

C. Mode III

This mode describes the turn-OFF process of the pulse generator. Unlike the discharge mode, there are some differences in this process under different types of loads. First, taking the resistive load as an example, as shown in Fig. 6(a), the discharge mode can be terminated when the switch M_4 turns OFF and D_8 will conduct forward at once. At the same time, the equivalent input capacitor C_{iss3} of M_3 and the energy-gaining capacitor C_{tr3} discharge through the loop of C_1–M_1–C_2–M_2–C_3–M_3–C_{iss3}–C_{tr3}–R_{Load}. Because $V_{Ciss3} + V_{Ctr3} = V_{diode8}$, M_3 will turn OFF when the voltage of the gate–source capacitor C_{gs3} of M_3 is lower than the threshold voltage, as shown in Fig. 7(a). The turn-OFF time of M_3 will be slightly longer than the turn-ON time since the threshold voltage of the switch is relatively low and the discharge time constant of C_{iss3} is greater than the charge time constant (C_4–C_{tr3}–C_{iss3}). Similarly, M_2 and M_1 will transit into the OFF state in sequence,

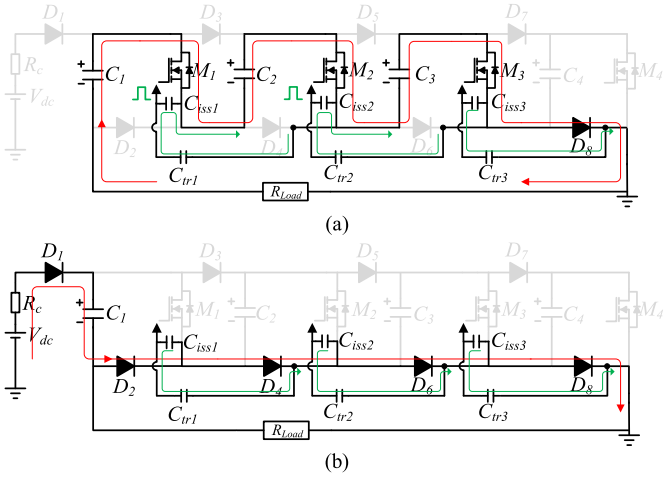

Fig. 6. (a) Turn-OFF transient state under a resistive load. (b) Turn-OFF mode under a resistive load.

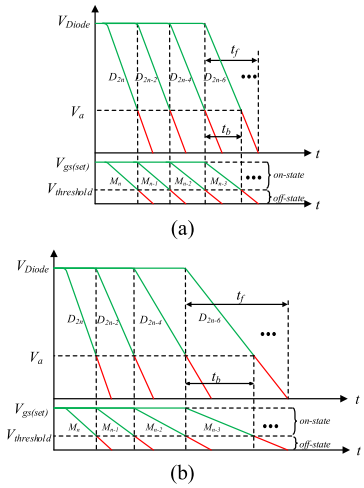

Fig. 7. Voltage diagrams of V_{Ciss} and V_{diode} (a) under a resistive load and (b) under a capacitive load.

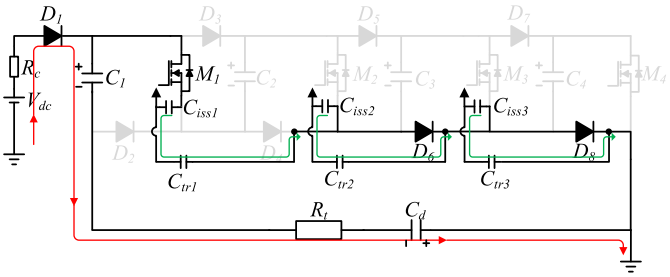

Fig. 8. Turn-OFF transient state under a capacitive load.

as shown in Fig. 6(b). Obviously, there is little difference in the turn-OFF delay of each switch under the resistive load.

If the type of load is capacitive, there will be residual voltage on the load capacitor after the end of Mode II. Taking the turn-OFF process of M_1 as an example, as shown in Fig. 8,

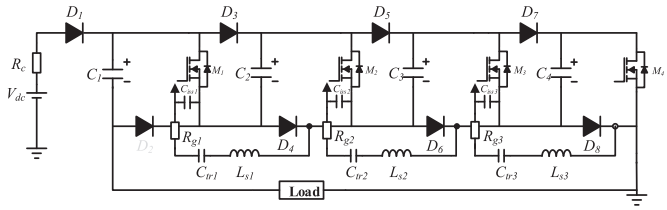

Fig. 9. Self-triggering Marx topology with stray parameters.

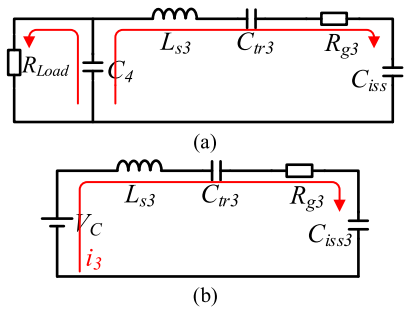

Fig. 10. (a) Gate trigger circuit of M_3. (b) Equivalent gate trigger circuit of M_3.

the residual charge of C_d will discharge through the loop V_{dc}–R_c–D_1–C_1–R_t–C_d, and the discharge time constant is relatively large, usually in the range of a few μs. D_4 cannot be conducted forward immediately if $V_{\mathrm{C1}} < V_{\mathrm{Cd}}$, which causes the turn-OFF time of M_1 to be prolonged. Similarly, the residual charge of C_d will lead the turn-OFF delay t_b of M_n, M_{n-1}, M_{n-2}, …, and to a gradual increase, as shown in Fig. 7(b).

III. Study on the Influence of Stray Parameters on the Switching Action Behavior

According to the previous analysis, the selection of the energy-gaining capacitor is crucial for the reliable turn-ON and turn-OFF of the switch. Moreover, the stray parameters of the trigger circuit branch have a great influence on the operating characteristics of the switch. Thus, this section will discuss these issues.

Fig. 9 illustrates the self-triggering Marx topology with stray inductance L_s in the trigger loop, where L_s is the sum of the stray inductances, including switches, capacitors, and line traces. It is worth noting that, in this study, the stray capacitance is not considered because the compact layout of the trigger loop makes the value of stray capacitance small enough to be negligible. To avoid large oscillations in the trigger loop, which may damage the switch, a drive resistor R_g is introduced here. After M_4 transitions into the ON state, the equivalent gate triggering circuit of M_3 is shown in Fig. 10(a). To simplify the analysis, assuming that during the discharge process, the voltage drop of the storage capacitor C_4 is small enough to be regarded as a dc power supply V_c. Hence, Fig. 10(a) can be equivalent to Fig. 10(b).

In fact, the triggering process of each MOSFET is a charge redistribution dynamic from the gate capacitors to the gate–source capacitor of each MOSFET. According to the principle of charge

conservation, the energy-gaining capacitor can be calculated by the following expression [30]:

$$C_{\mathrm{tr3(min)}} = \frac{Q}{\Delta U} = \frac{U_{gs(\mathrm{th})}C_{gs} + \left(U_{gs(\mathrm{th})} + U_{ds(\mathrm{OFF})}\right)C_{gd}}{U_{C4} - U_{gs(\mathrm{th})}} \approx \frac{U_{gs(\mathrm{th})}C_{gs} + U_{ds(\mathrm{OFF})}C_{gd}}{U_{C4}} \quad (1)$$

where $U_{gs(\mathrm{th})}$ and $U_{ds(\mathrm{OFF})}$ are the threshold voltage and drain–source voltage in the OFF state of M_3, respectively. Simultaneously, define a threshold voltage margin factor α, which satisfies

$$C_{\mathrm{tr3(max)}} \approx \frac{\alpha U_{gs(\mathrm{th})}C_{gs} + U_{ds(\mathrm{OFF})}C_{gd}}{U_{C4}} \quad (2)$$

where $U_{gs(\mathrm{set})} = \alpha U_{gs(\mathrm{th})} \le U_{gs(\mathrm{max})}$.

As long as C_{tr3} is within the range specified in (3), the generator can be triggered

$$C_{\mathrm{tr3(min)}} \le C_{\mathrm{tr3}} \le C_{\mathrm{tr3(max)}}. \quad (3)$$

The corresponding minimum output pulse voltage is

$$U_{p(\mathrm{min})} = nU_{gs_{(\mathrm{th})}}\frac{C_{\mathrm{tr3(max)}} + C_{gs}}{C_{\mathrm{tr3(max)}}}. \quad (4)$$

According to Fig. 10(b), it can be derived that

$$L_{s3}C_{\mathrm{iss3}}\frac{d^2u_{\mathrm{iss3}}}{dt^2} + R_gC_{\mathrm{iss3}}\frac{du_{\mathrm{iss3}}}{dt} + u_{\mathrm{iss3}} + \frac{C_{\mathrm{iss3}}}{C_{\mathrm{tr3}}}u_{\mathrm{iss3}} = V_C. \quad (5)$$

The characteristic root of (5) is

$$s_1 = -\frac{R_g}{2L_{s3}} + \sqrt{\frac{{R_g}^2}{4L^2{}_{s3}} - \frac{1}{L_{s3}C_{\mathrm{iss3}}}\left(1 + \frac{C_{\mathrm{iss3}}}{C_{\mathrm{tr3}}}\right)}$$

$$s_1 = -\frac{R_g}{2L_{s3}} - \sqrt{\frac{{R_g}^2}{4L^2{}_{s3}} - \frac{1}{L_{s3}C_{\mathrm{iss3}}}\left(1 + \frac{C_{\mathrm{iss3}}}{C_{\mathrm{tr3}}}\right)}. \quad (6)$$

To ensure that the switch can speed up the turn-ON and turn-OFF transition processes and avoid the emerging large voltage overshoot of the switch at the same time, which may damage the switch device, it is a good compromise to make the gate drive circuit work in the critical damping state, i.e.

$$\frac{{R_g}^2}{4L^2{}_{s3}} = \frac{1}{L_{s3}C_{\mathrm{iss3}}}\left(1 + \frac{C_{\mathrm{iss3}}}{C_{\mathrm{tr3}}}\right) \quad (7)$$

where

$$R_g = 2\sqrt{\frac{L_{s3}}{C_{\mathrm{iss3}}}\left(1 + \frac{C_{\mathrm{iss3}}}{C_{\mathrm{tr3}}}\right)}. \quad (8)$$

IV. Simulation Results

To verify the theoretical feasibility of the self-triggering nanosecond pulse generator proposed in this article, PSpice software is used for simulation verification, and the simulation parameters are shown in Table I.

The output pulse waveform of each stage under a resistive load is shown in Fig. 11. Figs. 12 and 13 show the pulse rising edge time and falling edge time of each stage, respectively. Clearly,

TABLE I
Simulation Parameters

Parameter	Value
Input DC voltage	V_{dc}=800 V
Number of modules	n=20
Voltage drop coefficient	α=10%
Pulse width	1 μs
Storage capacitor	C=0.8 F
Energy-gaining capacitor	C_{tr}=15 pF
Drive resistance	R_g=2.2 Ω
Resistive load	R_{load}=800 Ω
Capacitive Load	C_d=3 nF
Capacitive Load	R_t=800 Ω

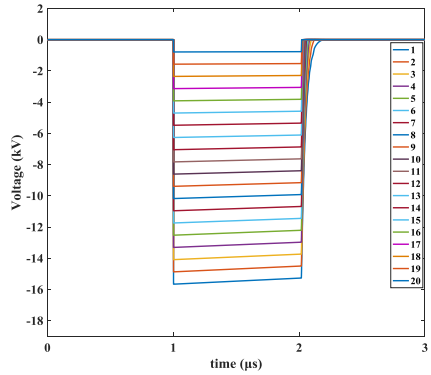

Fig. 11. Simulation superimposed output voltage waveform.

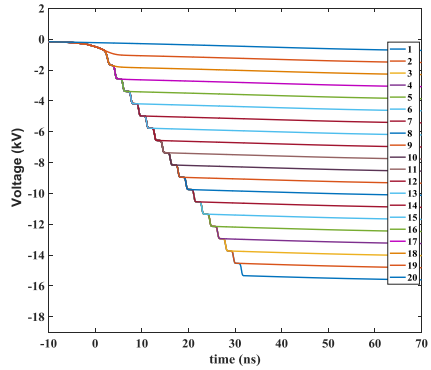

Fig. 12. Simulation rising edge voltage waveform.

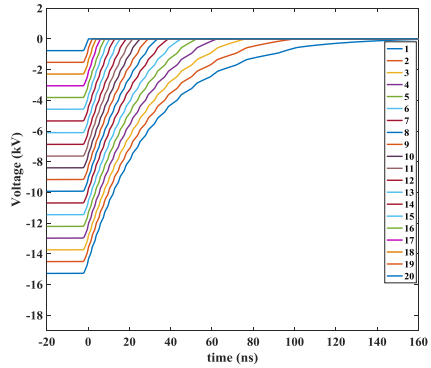

Fig. 13. Simulation falling edge voltage waveform.

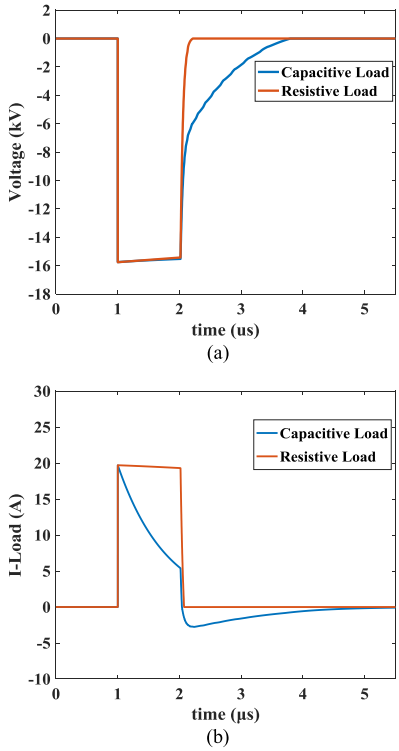

Fig. 14. Simulated waveforms under different loads. (a) Voltage waveforms. (b) Current waveforms.

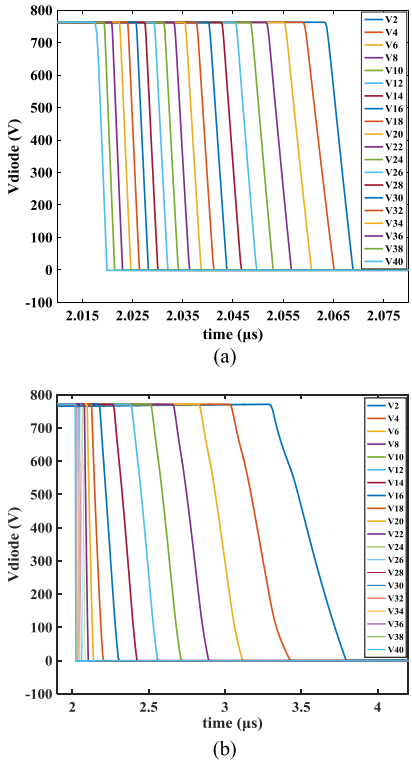

Fig. 15. Simulated voltage waveforms of V_{diode} under different loads. (a) Resistive load. (b) Capacitive load.

the falling edge of the output pulse is much slower than the rising edge. This phenomenon is not difficult to explain. First, since the switch has an output capacitor and a certain line inductance contained in the main discharge loop, the output capacitor needs to be charged after the discharge process finishes, and this process takes a certain time. Second, theoretically, there are only small driving resistors in the charging loop of the energy-gaining capacitor at all levels. However, a large load resistance was included in the discharge circuit, as shown in Figs. 3 and 6. As a result, the discharging time constant of the energy-gaining capacitor is larger than the charging time constant, and the turn-OFF delay between the stages is lengthened.

The voltage and current waveforms under a resistive load and a capacitive load are shown in Fig. 14. The tailing time of the falling edge of the pulse against the capacitive load is longer than that when against the resistive load. This behavior is because there is a certain residual charge on the load capacitor during the pulse, which causes D_{2n} of the corresponding stage to not immediately conduct forward. Therefore, the turn-OFF time of each switch is gradually prolonged. Fig. 15 illustrates the voltage waveforms of the turn-OFF transient across D_{2n} under the two types of load, which verify the above analysis.

In summary, the feasibility of the pulse generator topology proposed in this article is verified by simulation for different types of loads.

V. Experiment Results

It is necessary to optimize the printed circuit board (PCB) layout to minimize the size and weight of the pulse generator and achieve a more compact design with a higher voltage amplitude output. In this article, the PCB layout of the 20-stage superimposed self-triggered Marx pulse generator is provided, as shown in Fig. 16. The stray capacitance can be reduced by ensuring that the top and bottom discharge circuits do not overlap, and the stray inductance can be reduced by compact traces as far as possible. Then, a hardware prototype with the parameters in Table II is developed, as shown in Fig. 17. The size of the prototype is 5 cm $\times$ 1.2 cm $\times$ 40 cm, which meets the demands for the size and weight of the generator in some special application fields.

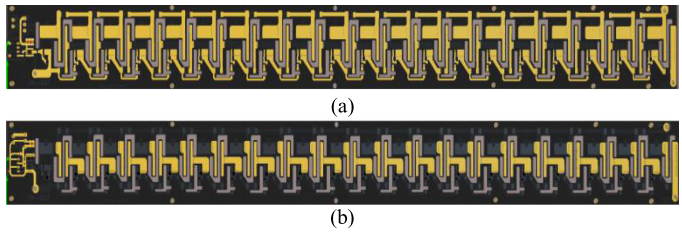

Fig. 16. (a) Discharge main circuit PCB of the top layer. (b) Discharge main circuit PCB of the bottom layer.

The drive waveform of the self-triggering switch with damping resistor R_g is shown in Fig. 18(a). R_g can significantly eliminate the shock of the drive loop. In addition, several stages of the self-trigger drive waveform are shown in Fig. 18(b). When the input voltage is equal to 800 V, the maximum setting value of the switching drive voltage in the steady state is $V_{gs(\mathrm{set})} =$ 10 V, which satisfies the design requirements.

TABLE II
PROTOTYPE PARAMETERS

Parameter	Value
Input DC voltage	V_{dc}=800 V
Number of modules	n=20
Voltage drop coefficient	α=10%
Storage capacitor	C=0.8 μF
Energy-gaining capacitor	C_{tr}=15 pF
Drive resistance	R_g=2.2 Ω
MOSFETs	C3M0065090J
Diode	HS5M
Resistive load	R_{load}=800 Ω
Capacitive load	C_d=3 nF
Capacitive load	R_t=800 Ω

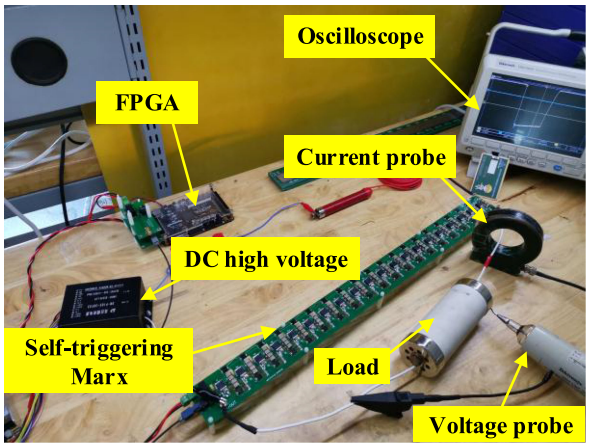

Fig. 17. Experimental prototype.

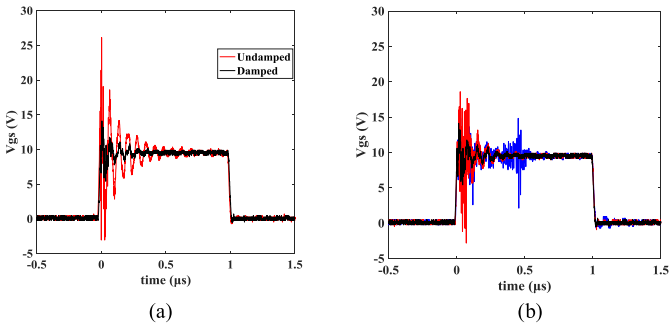

Fig. 18. (a) Undamped/damped drive waveform. (b) Drive waveform.

The typical output voltage waveform of the 20-stage self-triggering Marx generator is shown in Fig. 19. The maximum output voltage reaches 15.3 kV, with a 95.6% voltage conversion efficiency, and the pulse current amplitude is approximately 20 A. As shown in Fig. 19, there is no obvious oscillation emerging in the voltage and current waveforms, which fully verifies the stability of this generator.

Fig. 20 shows the voltage waveform of the pulse generator at a 10 kHz operating frequency in the form of a pulse train, confirming its reliability at a high operating frequency. Due to the output power limitation of a high-voltage dc source and a large charging protection resistor involved in the charge loop, there is a certain voltage difference between the output pulses.

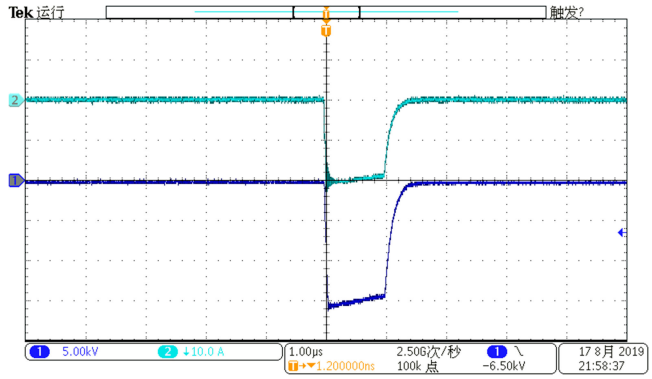

Fig. 19. Typical output voltage and current waveforms.

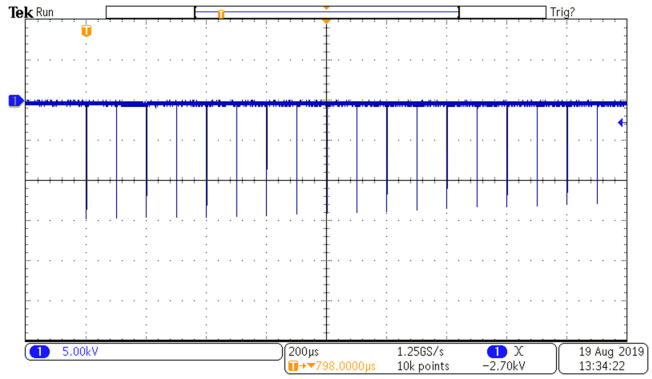

Fig. 20. Output voltage waveform with $f = 10$ kHz.

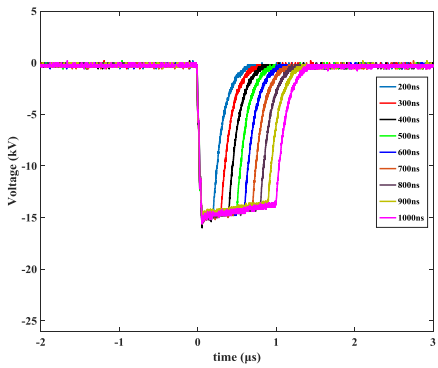

Fig. 21. Output voltage waveform with different widths.

Additionally, Fig. 21 illustrates the waveforms with widths ranging from 200 to 1000 ns. The pulse rising edge and the falling edge time with different pulsewidths are almost the same, which proves that the pulsewidth can be flexibly adjusted.

To investigate the dynamic superimposed output waveform characteristics of the 20-stage self-triggering Marx pulse generator, a pictorial diagram showing the voltages across each stage is shown in Fig. 22(a). It is worth noting that only voltage waveforms of the previous five stages are measured here, limited by the common voltage withstand capability of a high-voltage differential probe. Additionally, the output voltage of 20 stages

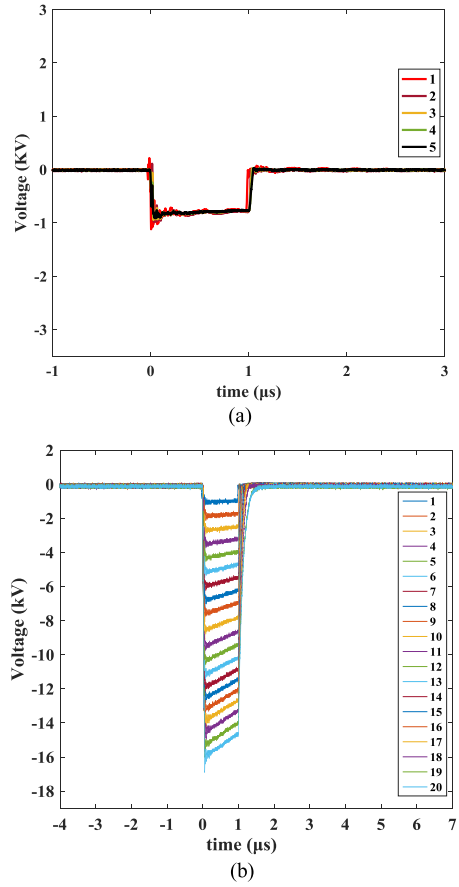

Fig. 22. (a) Voltage waveforms across the previous five stages. (b) Superimposed output voltage waveform of the 20 stages.

is tested gradually, as shown in Fig. 22(b). The high power output is achieved through the cascade mode of the Marx structure.

Fig. 23(a) illustrates the rising edge waveform of the 20-stage output pulse with an 800-Ω resistive load, and the rising time (10%–90%) is approximately 45 ns. It is remarkable that the typical rising time of C3M0065090J is approximately 15 ns. Although the rising edge of the output pulse is slower than the switch itself, it is not serious. Fig. 23(b) shows the rising edge waveform of the output pulse with a 10-kΩ resistance load. Comparing Fig. 23(a) and (b), it can be found that the rising edge oscillation of the output pulse is increased under the 800-Ω load. This increase is mainly because there are some unavoidable stray inductances in the discharge loop, and the reduction of R_{Load} will increase the influence of the stray inductance, leading to the aggravation of the oscillation. In addition, the pulse rising edge waveforms of the prototype under the resistive load (R_{Load} = 800 Ω) and the capacitive load ($C_d = 3\,\mathrm{nF}$, $R_t = 800\,\Omega$) are shown in Fig. 23(c). When the relaxation time of the load changes, the rising time of the pulse is basically the same, which indicates that the pulse generator has a good leading edge characteristic.

Fig. 24 shows the falling edge waveform of the 20-stage output pulse with different loads. The falling time (10%–90%) is approximately 280 ns when the load is equal to 800 Ω, whereas the fall time is approximately 1.6 μs under a 10-kΩ load. The

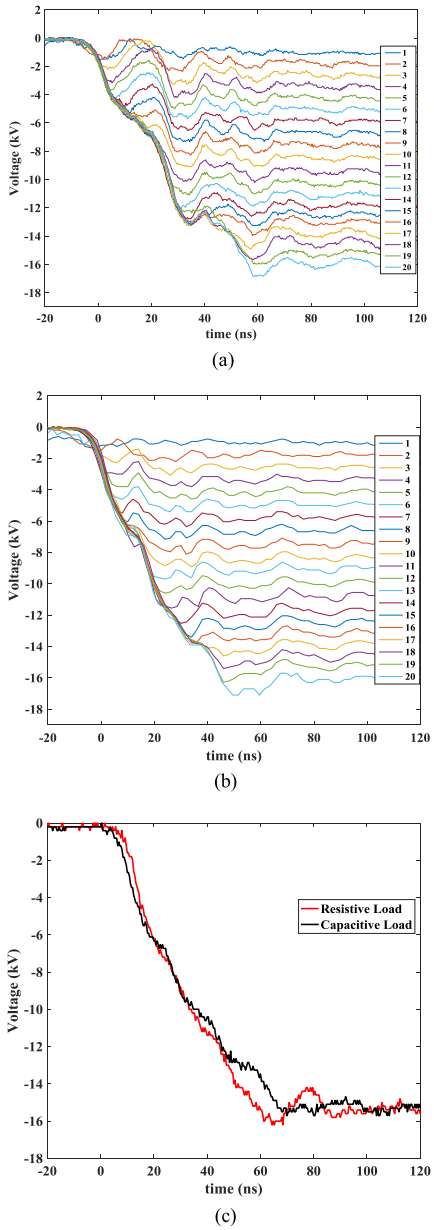

Fig. 23. Output pulse rising edge waveform with different loads. (a) $R_{\mathrm{Load}} =$ 800 Ω. (b) $R_{\mathrm{Load}} = 10$ kΩ. (c) Resistive and capacitive loads.

increase in R_{Load} will significantly delay the falling edge of the output pulse. When the pulse generator operates under a capacitive load, the pulse waveform is shown in Fig. 24(c). It is obvious that the falling edge of the pulse under a capacitive load is much slower than that under a resistive load. Detailed reasons have been described previously. This result indicates that the type of load has a greater influence on the falling edge compared to the rising edge. Fortunately, in the dielectric barrier plasma discharge, the particle activity and generation efficiency are mainly determined by the pulse rising edge time and the pulse voltage amplitude.

Fig. 25. Pulse current waveform of the pulse generator under a resistive load ($R_{\mathrm{Load}} = 800\ \Omega$) and a capacitive load ($C_d =$ 3 nF, $R_t = 800\,\Omega$), and the current amplitude is up to 20 A.

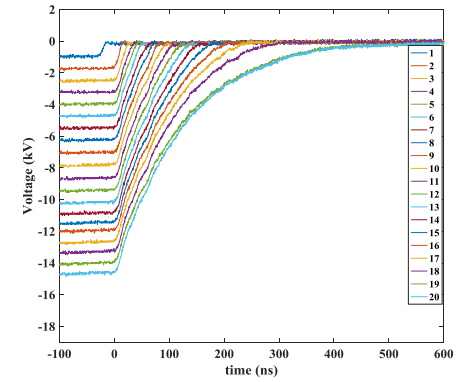

(a)

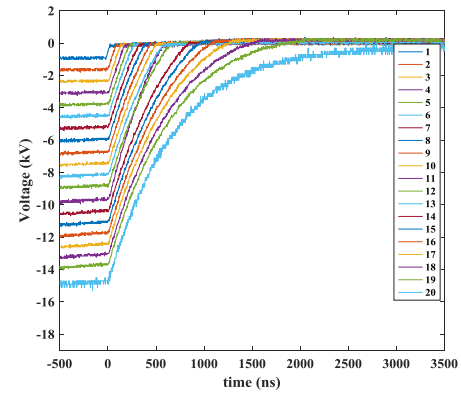

(b)

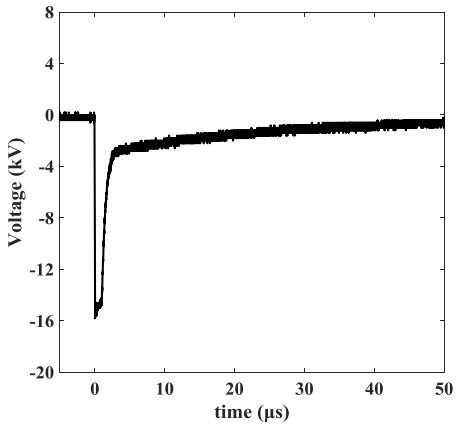

(c)

Fig. 24. Output pulse falling edge waveform with different loads. (a) $R_{\mathrm{Load}} = 800\ \Omega$. (b) $R_{\mathrm{Load}} = 10\ \mathrm{k}\Omega$. (c) Capacitive load.

As mentioned above, the self-triggering Marx pulse generator proposed in this article does not have the problem of switching voltage equalization. Fig. 26 visually shows the drain–source voltage waveform of several MOSFETs among them. Clearly, the drain–source voltages of different MOSFETs are basically equal on the switching transients. Therefore, the same type of switch can be employed at all stages, which can be used close to the fully rated value. This conclusion is consistent with the previous analysis.

Generally, the experimental results prove the feasibility and practicability of the topology of Fig. 1(a).

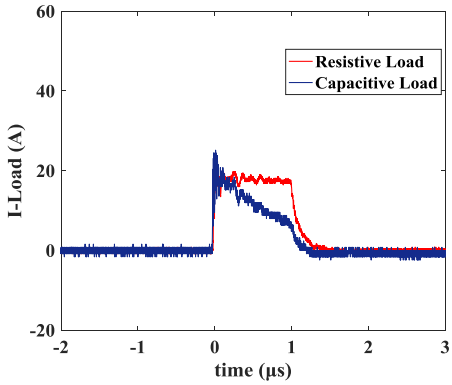

Fig. 25. Current waveforms under different loads.

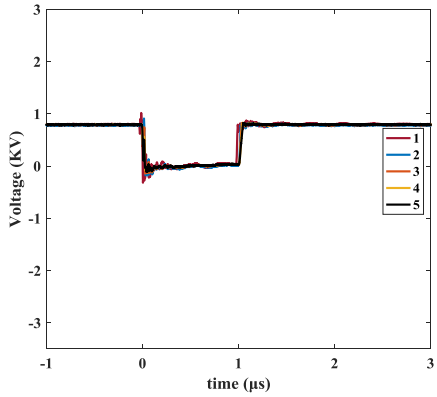

Fig. 26. Drain–source voltage waveform of the MOSFET.

VI. Conclusion

In this article, a novel all solid-state high-voltage repetition nanosecond self-triggering Marx pulse generator is developed, and the following conclusions are drawn.

1) Based on the high potential-energy-gaining technology of the interstage capacitors, a compact self-triggering Marx pulse generator is studied. This generator possesses the following advantages. The complex isolated driving problem of the switches during discharge of the classical Marx topology has been solved. Theoretically, the number of stages can be expanded arbitrarily to obtain a high-voltage gain pulse output. Moreover, there is no isolation withstand voltage limitation, which greatly reduces the size and weight of the device.
2) Based on the classical Marx topology, switches at all stages bear the same voltage either in the ON-state or OFF-state transient, and there is no longer dynamic and static voltage sharing problems, which ensures long-term reliable operation of the switch with safe voltages.
3) At present, the output parameters obtained are as follows. The frequency in the pulse train is 10 kHz, the pulsewidth is 200–1000 ns, and the pulse voltage amplitude reaches 15.3 kV with a rising time of approximately 45 ns.

In summary, this novel generator has a compact structure, a rapid rising time, flexible output waveform parameters, and an

adjustable pulsewidth in the range of hundreds of nanoseconds, which can easily increase the voltage level. There are good application prospects in plasma flow control and plasma-assisted combustion.

REFERENCES

[1] H. Du *et al.*, "The study of flow separation control by a nanosecond pulse discharge actuator," *Exp. Thermal Fluid Sci.*, vol. 74, pp. 110–121, 2016.

[2] D. Hai *et al.*, "Topological structures of vortex flow on a flying wing aircraft, controlled by a nanosecond pulse discharge plasma actuator," *App. Phys. Lett.*, vol. 108, no. 24, 2016, Art. no. 244105.

[3] S. J. Pendleton, J. Kastner, E. Gutmark, and M. A. Gundersen, "Surface streamer discharge for plasma flow control using nanosecond pulsed power," *IEEE Trans. Plasma Sci.*, vol. 39, no. 11, pp. 2072–2073, Nov. 2011.

[4] E. Pescini, L. Francioso, M. G. D. Giorgi, and A. Ficarella, "Investigation of a micro dielectric barrier discharge plasma actuator for regional aircraft active flow control," *IEEE Trans. Plasma Sci.*, vol. 43, no. 10, pp. 3668–3680, Oct. 2015.

[5] D. V. Roupassov, A. A. Nikipelov, M. M. Nudnova, and A. Y. Starikovskii, "Flow separation control by plasma actuator with nanosecond pulse periodic discharge," in *Proc. Int. Conf. Gas Discharges App.*, 2009, pp. 609–612.

[6] E. Moreau, A. Debien, N. Benard, and N. J. Zouzou, "Nanosecond-pulsed dielectric barrier discharge plasma actuator for airflow control along an NACA0015 airfoil at high Reynolds number," *IEEE Trans. Plasma Sci.*, vol. 44, no. 11, pp. 1–9, Nov. 2016.

[7] A. Y. Starikovskii, A. A. Nikipelov, M. M. Nudnova, and D. V. Roupassov, "SDBD plasma actuator with nanosecond pulse-periodic discharge," *Plasma Sources Sci. Technol.*, vol. 18, no. 3, 2009, Art. no. 034015.

[8] J. P. M. Mendes, H. Canacsinh, L. M. Redondo, and J. O. Rossi, "Solid state Marx modulator with Blumlein stack for bipolar pulse generation," *IEEE Trans. Dielectr. Elect. Insul.*, vol. 18, no. 4, pp. 1199–1204, Aug. 2011.

[9] Y. Mi, C. Bian, P. Li, C. Yao, and C. Li, "A modular generator of nanosecond pulses with adjustable polarity and high repetition rate," *IEEE Trans. Power Electron.*, vol. 33, no. 12, pp. 10654–10662, Dec. 2018.

[10] Y. Liang, Z. Jiu, T. Sugai, A. Tokuchi, and W. J. Jiang, "Pulsed voltage adder topology based on inductive Blumlein lines," *IEEE Trans. Plasma Sci.*, vol. 46, no. 5, pp. 1816–1820, May 2018.

[11] Y. Liu, R. Fan, X. Zhang, Z. Tu, and J. Zhang, "Bipolar high voltage pulse generator without H-bridge based on cascade of positive and negative Marx generators," *IEEE Trans. Dielectr. Elect. Insul.*, vol. 26, no. 2, pp. 476–483, Apr. 2019.

[12] T. Sakamoto, A. Nami, M. Akiyama, and H. Akiyama, "A repetitive solid state Marx-type pulsed power generator using multistage switch-capacitor cells," *IEEE Trans. Plasma Sci.*, vol. 40, no. 10, pp. 2316–2321, Oct. 2012.

[13] X. Lan, M. Long, X. Zi-Jie, X. Qin, Z. De-Qing, and Y. Zi-Kang, "A novel generator for high-voltage bipolar square pulses with applications in sterilization of microorganism," *IEEE Trans. Dielectr. Elect. Insul.*, vol. 22, no. 4, pp. 1887–1895, Aug. 2015.

[14] R. Khosravi and M. Rezanejad, "A new pulse generator with high voltage gain and reduced components," *IEEE Trans. Ind. Electron.*, vol. 66, no. 4, pp. 2795–2802, Apr. 2019.

[15] M. A. Elgenedy, A. Darwish, S. Ahmed, and B. W. Williams, "A transition arm modular multilevel universal pulse-waveform generator for electroporation applications," *IEEE Trans. Power Electron.*, vol. 32, no. 12, pp. 8979–8991, Dec. 2017.

[16] A. Darwish, M. A. Elgenedy, S. J. Finney, B. W. Williams, and J. R. McDonald, "A step-up modular high-voltage pulse generator based on isolated input-parallel/output-series voltage-boosting modules and modular multilevel submodules," *IEEE Trans. Ind. Electron.*, vol. 66, no. 3, pp. 2207–2216, Mar. 2019.

[17] W. Jiang, "Solid-state LTD module using power MOSFETs," *IEEE Trans. Plasma Sci.*, vol. 38, no. 10, pp. 2730–2733, Oct. 2010.

[18] M. R. Kazemi, T. Sugai, A. Tokuchi, and W. Jiang, "Waveform control of pulsed-power generator based on solid-state LTD," *IEEE Trans. Plasma Sci.*, vol. 45, no. 2, pp. 247–251, Feb. 2017.

[19] C. Yao, S. Dong, Y. Zhao, M. Yan, and C. J. Li, "A novel configuration of modular bipolar pulse generator topology based on Marx generator with double power charging," *IEEE Trans. Plasma Sci.*, vol. 44, no. 10, pp. 1872–1878, Oct. 2016.

[20] X. Ren, Z.-W. Xu, K. Xu, Z. Zhang, and Q. Chen, "SiC stacked-capacitor converters for pulse applications," *IEEE Trans. Power Electron.*, vol. 34, no. 5, pp. 4450–4464, May 2019.

[21] C.-H. Yu, S.-R. Jang, H.-S. Kim, and H.-J. Ryoo, "Gate driving circuit with active pull-down function for a solid-state pulsed power modulator," *IEEE Trans. Power Electron.*, vol. 33, no. 1, pp. 240–247, Jan. 2018.

[22] Z. Li, H. Liu, S. Jiang, and J. Rao, "A novel drive circuit with overcurrent protection for solid state pulse generators," *IEEE Trans. Dielectr. Elect. Insul.*, vol. 26, no. 2, pp. 361–366, Apr. 2019.

[23] S.-R. Jang, C.-H. Yu, and H.-J. Ryoo, "Simplified design of a solid state pulsed power modulator based on power cell structure," *IEEE Trans. Ind. Electron.*, vol. 65, no. 3, pp. 2112–2121, Mar. 2018.

[24] Y. Wang, L. Tong, K. Liu, and Y. Huang, "Repetitive high-voltage pulse modulator using bipolar Marx generator combined with pulse transformer," *IEEE Trans. Plasma Sci.*, vol. 46, no. 10, pp. 3340–3347, Oct. 2018.

[25] S. Liu and M. J. Neiger, "Electrical modelling of homogeneous dielectric barrier discharges under an arbitrary excitation voltage," *J. Phys. D, App. Phys.*, vol. 36, no. 24, 2003, Art. no. 3144.

[26] L. Pang, T. Long, K. He, Y. Huang, and Q. Zhang, "A compact series-connected SiC MOSFETs module and its application in high voltage nanosecond pulse generator," *IEEE Trans. Ind. Electron.*, vol. 66, no. 12, pp. 9238–9247, Dec. 2019.

[27] W. Jiang, H. Sugiyama, and A. Tokuchi, "Pulsed power generation by solid-state LTD," *IEEE Trans Plasma Sci.*, vol. 42, no. 11, pp. 3603–3608, Nov. 2014.

[28] J. Rao, W. Zhang, S. Jiang, Z. Li, and E. Insulation, "Nanosecond pulse generator based on cascaded avalanche transistors and Marx circuits," *IEEE Trans. Dielectr. Elect. Insul.*, vol. 26, no. 2, pp. 374–380, Apr. 2019.

[29] J. T. Li *et al.*, "Development of a stereo-symmetrical nanosecond pulsed power generator composed of modularized avalanche transistor Marx circuits," *Rev. Sci. Instrum.*, vol. 86, no. 9, 2015, Art. no. 093502.

[30] B. J. Baliga, *Fundamentals of Power Semiconductor Devices*. New York, NY, USA: Springer, 2012.

Weirong Zeng was born in Chongqing, China, in 1995. He received the B.Sc. degree from China University of Petroleum, Qingdao, China, in 2018. He is currently working toward the Ph.D. degree with the Department of Electrical Engineering, Chongqing University, Chongqing, China.

His research interests include pulse power technology and new technologies of electrical engineering in biomedicine and its treatment apparatus.

Chenguo Yao (Member, IEEE) was born in Nanchong, Sichuan, China. He received the B.S., M.S., and Ph.D. degrees from Chongqing University, Chongqing, China, in 1997, 2000, and 2003, respectively, all in electrical engineering.

He became a Professor with the College of Electrical Engineering, Chongqing University, in 2007. His current research interests include pulse power technology and its application in biomedical engineering, online monitoring of insulation condition, and insulation fault diagnosis for HV apparatus.

Shoulong Dong (Member, IEEE) was born in Taian, Shandong, China, on December 2, 1989. He received the B.S. and Ph.D. degrees from Chongqing University, Chongqing, China, in 2011 and 2017, respectively, all in electrical engineering.

He is currently a Lecturer with the School of Electrical Engineering, Chongqing University. His research interests include pulse power technology and new technologies of electrical engineering in biomedicine and its treatment apparatus.

Yilin Wang was born in Chongqing, China, in 1995. He received the B.S. degree in electrical engineering in 2017 from Chongqing University, Chongqing, China, where he is currently working toward the M.S. degree in electrical engineering.

His research interests include pulse power technology and new technologies of electrical engineering in biomedicine and its treatment apparatus.

Jianhao Ma (Student Member, IEEE) was born in Hengdian, Zhejiang, China, on December 23, 1993. He received the B.S. degree in electrical engineering from Guangxi University, Nanning, China, in 2016. He is currently working toward the Ph.D. degree in electrical engineering with Chongqing University, Chongqing, China.

His research interests include pulse power technology, and developing new biomedical technologies and treatment apparatus through electrical engineering.

Yingjiang He was born in Sichuan, China, in 1995. He received the B.S. degree from China University of Petroleum, Qingdao, China, in 2018. He is currently working toward the M.S. degree in electrical engineering with Chongqing University, Chongqing, China.

His research interest includes high-repetition-rate pulse power technology and its applications.

Liang Yu (Member, IEEE) was born in Wuhan, Hubei, China, in 1986. He received the Ph.D. degree from Nagaoka University of Technology, Nagaoka, Japan, in 2018.

He is currently an Assistant Professor with Chongqing University, Chongqing, China. His main directions are pulse power technology and its applications, high-power semiconductor device applications, and bioelectrotechnical technology and its applications.